PERGAMON

International Journal of Solids and Structures 38 (2001) 9505–9523

INTERNATIONAL JOURNAL OF SOLIDS and STRUCTURES

www.elsevier.com/locate/ijsolstr

A theoretical and computational framework for anisotropic continuum damage mechanics at large strains

A. Menzel, P. Steinmann *

Chair of Applied Mechanics, University of Kaiserslautern, P.O. Box 3049, D-67653 Kaiserslautern, Germany

Received 13 October 1999; in revised form 7 September 2000

Abstract

The main objective of this work is the formulation and algorithmic treatment of anisotropic continuum damage mechanics at large strains. Based on the concept of a fictitious, isotropic, undamaged configuration an additional linear tangent map is introduced which allows the interpretation as a damage deformation gradient. Then, the corresponding Finger tensor – denoted as damage metric – constructs a second order, internal variable. Due to the principle of strain energy equivalence with respect to the fictitious, effective space and the standard reference configuration, the free energy function can be computed via push-forward operations within the nominal setting. Referring to the framework of standard dissipative materials, associated evolution equations are constructed which substantially affect the anisotropic nature of the damage formulation. The numerical integration of these ordinary differential equations is highlighted whereby two different schemes and higher order methods are taken into account. Finally, some numerical examples demonstrate the applicability of the proposed framework. © 2001 Elsevier Science Ltd. All rights reserved.

Keywords: Continuum damage mechanics; Anisotropy; Finite deformations; Time integration

1. Introduction

To capture the anisotropic nature of damage one has at least to introduce a second order internal variable, see e.g. Leckie and Onat (1981). Hence the main goal of this contribution is the development of a framework for geometrically non-linear, anisotropic, tensorial second order continuum damage. Anisotropy – already within the purely elastic case – comes into the picture if the introduced second order internal variable is not a spherical one. Additionally, depending on the corresponding rate equations, the categories of quasi-isotropic and anisotropic damage evolution are classified.

In order to formulate tensorial second order continuum damage we make use of the concept of a fictitious, undamaged configuration, see e.g. Betten (1982) and Murakami (1988) or the recent publication of Park and Voyiadjis (1998). This fictitious space corresponds to the effective space of the classical [1-D]

* Corresponding author. Address: Department of Mechanical Engineering, University of Kaiserslautern, Erwin-Schroedinger-Strasse, Gebaeude 44, D-67653 Kaiserslautern, Germany. Tel.: +49-631-205-2419; fax: +49-631-205-2128.

E-mail address: ps@rhrk.uni-kl.de (P. Steinmann).

0020-7683/01/$ - see front matter
PII: S0020-7683(01)00136-6

damage theory. Nevertheless, this second order approach deals with a stored strain energy based on the effective or nominal space, respectively, whereby the damage metric acts on the strain metric as developed by Steinmann and Carol (1998). Furthermore, the proposed anisotropic framework is directly based on the theory of standard dissipative materials. This formalism consequently leads to the introduction of an elastic domain, the postulate of maximum dissipation and associated evolution equations. In case of anisotropy these rate equations represent a reduced set compared to a general tensor-valued tensor function in terms of e.g. the strain metric and internal variables; see Betten (1985). A main advantage of the proposed formulation is the opportunity to use standard isotropic hyper-elastic constitutive equations in terms of the nominal strain and damage metric to formulate anisotropic material behavior.

Concerning the numerical integration of the evolution equations with respect to higher order, Runge–Kutta methods two different categories of algorithms are classified. Namely, within the first category only the actual configuration is forced to stay in the elastic domain whereby the second category additionally demands the algorithmic intermediate stages to fulfil this condition. The algorithmic treatment is straightforward and several implicit and explicit Runge–Kutta algorithms of different order are outlined; for a survey see e.g. Lambert (1991) or the textbook of Ascher and Petzold (1998) and references cited therein. Both categories are applied within a staggered formulation on a local level.

Finally, as a first illustration of the developed framework and for comparison of different integration algorithms, numerical examples with respect to homogeneous deformations conclude this contribution.

2. Continuum mechanical framework

This section summarizes some basics of non-linear continuum mechanics within the setting of a multiplicative composition with respect to the standard elastic deformation gradient and a damage mapping following the framework given in Steinmann and Carol (1998). Due to the general anisotropic character it is self-evident to base the formulation on a material setting in terms of an appropriate set of invariants. For a large strain isotropic continuum damage formulation which is numerically based on the computation of eigenvalues and generally formulated within the spatial setting see e.g. Miehe (1995). Later on, the well established theory of standard dissipative materials is consequently applied. Appendix A additionally states some notation used in the sequel.

2.1. Basic kinematics and metric tensors

As usual, the considered body within the standard reference configuration is denoted by $\mathscr{B}_0 \subset \mathbb{R}^3$ and $\boldsymbol{x} = \boldsymbol{\varphi}(\boldsymbol{X})$ represents the standard non-linear elastic deformation map of material points $\boldsymbol{X} \in \mathscr{B}_0$ onto spatial points $\boldsymbol{x} \in \mathscr{B}$ in the current configuration $\mathscr{B} \subset \mathbb{R}^3$. The corresponding linear map – introduced as deformation gradient – $\boldsymbol{F} = \partial_{\boldsymbol{X}} \boldsymbol{\varphi}$: $\mathscr{T}\mathscr{B}_0 \to \mathscr{T}\mathscr{B}$ with $\det \boldsymbol{F} > 0$ transforms tangent vectors of material curves into tangent vectors of spatial curves.

Similar to $\boldsymbol{F}$ an additional linear map $\bar{\boldsymbol{F}}$: $\mathscr{T}\bar{\mathscr{B}}_0 \to \mathscr{T}\mathscr{B}_0$ is introduced, whereby $\det \bar{\boldsymbol{F}} > 0$ is assumed throughout, compare Steinmann and Carol (1998). Furthermore, the linear mapping $\bar{\boldsymbol{F}}$ allows the interpretation as superposed diffeomorphism. Within the light of continuum damage the corresponding space $\bar{\mathscr{B}}_0$ represents a fictitious, undamaged reference configuration – often denoted as effective space, see Fig. 1 for a symbolic, graphical representation.

The change of length of line elements as a consequence of the deformation of the body of interest is represented by the Almansi strain tensor $\boldsymbol{e} \in \mathscr{B}$ and the Green–Lagrange strain tensor $\boldsymbol{E} \in \mathscr{B}_0$, respectively. Their interpretation from differential geometry is given by the differences of covariant metric tensors. Thus, these tensors will often be referred to as strain metrics in the following. Next, standard pull-back operations with the fictitious damage mapping $\bar{\boldsymbol{F}}$ applied to $\boldsymbol{E}$ yields the effective strain metric in $\bar{\mathscr{B}}_0$

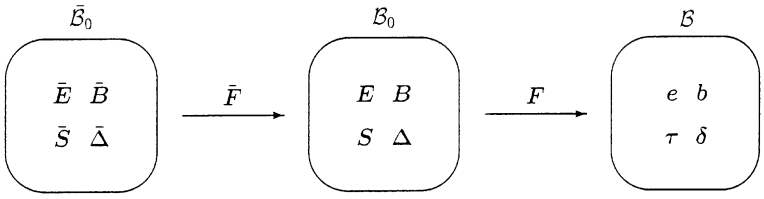

Fig. 1. Strain metric, damage metric and conjugate stresses with respect to the fictitious, isotropic reference configuration $\bar{\mathcal{B}}_0$, the standard reference configuration $\mathcal{B}_0$ and the spatial setting $\mathcal{B}$.

$$\boldsymbol{e} \in \mathcal{B}, \quad \boldsymbol{E} = \boldsymbol{F}^{\mathrm{T}} \cdot \boldsymbol{e} \cdot \boldsymbol{F} \in \mathcal{B}_0, \quad \bar{\boldsymbol{E}} = \bar{\boldsymbol{F}}^{\mathrm{T}} \cdot \boldsymbol{E} \cdot \bar{\boldsymbol{F}} \in \bar{\mathcal{B}}_0. \tag{1}$$

In order to compute the scalar-valued free energy function Ψ a second order, contravariant metric tensor is used, whereby again standard pull-back and push-forward operations hold

$$\bar{\boldsymbol{B}} \in \bar{\mathcal{B}}_0, \quad \boldsymbol{B} = \bar{\boldsymbol{F}} \cdot \bar{\boldsymbol{B}} \cdot \bar{\boldsymbol{F}}^{\mathrm{T}} \in \mathcal{B}_0, \quad \boldsymbol{b} = \boldsymbol{F} \cdot \boldsymbol{B} \cdot \boldsymbol{F}^{\mathrm{T}} \in \mathcal{B}, \tag{2}$$

compare Fig. 1 for a graphical visualization. These symmetric, positive definite tensors $\bar{\boldsymbol{B}}$, $\boldsymbol{B}$ and $\boldsymbol{b}$ can be interpreted initially as energy metrics; e.g. $\boldsymbol{B} \in \mathcal{B}_0$ is one to one with the inverse of the standard covariant metric tensor $\boldsymbol{G}^{-1} \in \mathcal{B}_0$. Nevertheless, we tend to denote the metric tensors due to Eq. (2) as damage metrics in the sequel since they will come into the picture as internal damage variables. For a constitutive framework to formulate anisotropic elasto-plasticity at large strains in terms of a plastic metric we refer to Miehe (1998).

Furthermore, the heart of the proposed formulation lies in the supposition $\bar{\boldsymbol{B}} \doteq \bar{\boldsymbol{I}}$ which consequently leads to the physical interpretation of $\bar{\mathcal{B}}_0$ as an undamaged, isotropic, fictitious reference configuration. Hence, in the case of damage evolution the eigenvalues ${}^{B}\lambda$ with respect to $\boldsymbol{B}$ are degrading, which means ${}^{B}\lambda < 0$.

2.2. Strain energy equivalence

Due to the principle of strain energy equivalence the free energy function Ψ per unit volume in $\mathcal{B}_0$ can be computed within the fictitious –, the standard reference –, or the current configuration, respectively

$$\bar{\Psi}(\bar{\boldsymbol{E}}, \bar{\boldsymbol{B}}) = \Psi(\boldsymbol{E}, \boldsymbol{B}) = \psi(\boldsymbol{e}, \boldsymbol{b}), \tag{3}$$

here in terms of the internal damage variable and the corresponding strain tensor.

Generally, a tensor function defined by two symmetric, second order tensors is represented by a set of 10 invariants, see e.g. Spencer (1971). Thus, Eq. (3) is one to one with $\bar{\Psi}({}^{\bar{E}\bar{B}}\widetilde{I}_i) = \Psi({}^{EB}\widetilde{I}_i) = \psi({}^{eb}\widetilde{I}_i)$ for $i = 1, \ldots, 10$. Restriction to an isotropic configuration $\bar{\mathcal{B}}_0$ with $\bar{\boldsymbol{B}} \doteq \bar{\boldsymbol{I}}$ yields $i = 1, 2, 3$ and straightforward the basic invariants

$${}^{\bar{E}\bar{B}}I_1 = \bar{\boldsymbol{E}}{:}\bar{\boldsymbol{B}}, \quad {}^{\bar{E}\bar{B}}I_2 = [\bar{\boldsymbol{E}} \cdot \bar{\boldsymbol{B}} \cdot \bar{\boldsymbol{E}}]{:}\bar{\boldsymbol{B}}, \quad {}^{\bar{E}\bar{B}}I_3 = [\bar{\boldsymbol{E}} \cdot \bar{\boldsymbol{B}} \cdot \bar{\boldsymbol{E}} \cdot \bar{\boldsymbol{B}} \cdot \bar{\boldsymbol{E}}]{:}\bar{\boldsymbol{B}}. \tag{4}$$

Accordingly, within the standard reference configuration $\mathcal{B}_0$ the set of invariants reads

$${}^{EB}I_1 = \boldsymbol{E}{:}\boldsymbol{B}, \quad {}^{EB}I_2 = [\boldsymbol{E} \cdot \boldsymbol{B} \cdot \boldsymbol{E}]{:}\boldsymbol{B}, \quad {}^{EB}I_3 = [\boldsymbol{E} \cdot \boldsymbol{B} \cdot \boldsymbol{E} \cdot \boldsymbol{B} \cdot \boldsymbol{E}]{:}\boldsymbol{B}. \tag{5}$$

This emphasizes that anisotropic continuum damage is formulated just by replacing the set of basic invariants in the free energy function which is the central idea of the proposed framework. As a main advantage, standard isotropic free energy functions can be used to model anisotropic damage. For a general overview on the construction of constitutive equations for anisotropic materials see Smith (1994).

Note that within the initially elastic domain isotropy is included if $\bar{\boldsymbol{F}}$ is a spherical tensor. Alternative approaches to formulate anisotropy applying an enhanced right stretch tensor $\boldsymbol{U}$ have been proposed by Ogden (1997) and Sansour (1999). Whether the damage formulation itself is anisotropic or not only depends on the chosen evolution equation of the damage metric. Since the internal damage variable is introduced as a second order tensor typical classes of anisotropic materials like transverse isotropy and orthotropy are implied in this framework which is underlined by the spectral decomposition of $\boldsymbol{B} \in \mathscr{B}_0$

$$\boldsymbol{B} = \sum_{i=1}^{3} {}^{B}\lambda_i \, {}^{B}\boldsymbol{n}_i \otimes {}^{B}\boldsymbol{n}_i \doteq \alpha_0 \boldsymbol{I} + \alpha_1 \, {}^{B}\boldsymbol{n}_1 \otimes {}^{B}\boldsymbol{n}_1 + \alpha_2 \, {}^{B}\boldsymbol{n}_2 \otimes {}^{B}\boldsymbol{n}_2, \tag{6}$$

as pointed out by Svendsen (2001).

Example 2.1. To show the parallelism between the considered fictitious map and structural tensors as e.g. used by Spencer (1984) to formulate transverse isotropy and orthotropy three different types of mappings $\bar{\boldsymbol{F}}$ are outlined which compute $\boldsymbol{B} = \bar{\boldsymbol{F}} \cdot \bar{\boldsymbol{B}} \cdot \bar{\boldsymbol{F}}^{\mathrm{T}}$ for $\bar{\boldsymbol{B}} \doteq \bar{\boldsymbol{I}}$ keeping the notation of Eq. (6) in mind:

Isotropy: For a spherical damage mapping with $\bar{\boldsymbol{F}} = \beta_0 \boldsymbol{I}$ the damage metric $\boldsymbol{B}$ is defined by $\alpha_0 = \beta_0^2$, $\alpha_1 = 0$ and $\alpha_2 = 0$.

Transverse Isotropy: Enlarging this spherical mapping by a rank one term of the form $\bar{\boldsymbol{F}} = \beta_0 \boldsymbol{I} + \beta_1 \, {}^{B}\boldsymbol{n}_1 \otimes {}^{B}\boldsymbol{n}_1$ renders $\alpha_0 = \beta_0^2$, $\alpha_1 = 2\beta_0\beta_1 + \beta_1^2$ and $\alpha_2 = 0$.

Orthotropy: Finally, an additional dyadic constructs $\bar{\boldsymbol{F}} = \beta_0 \boldsymbol{I} + \beta_1 \, {}^{B}\boldsymbol{n}_1 \otimes {}^{B}\boldsymbol{n}_1 + \beta_2 \, {}^{B}\boldsymbol{n}_2 \otimes {}^{B}\boldsymbol{n}_2$ yielding $\alpha_0 = \beta_0^2$, $\alpha_1 = 2\beta_0\beta_1 + \beta_1^2$ and $\alpha_2 = 2\beta_0\beta_2 + \beta_2^2$.

Remark 2.1. Without danger of confusion the general set of 10 invariants defined by two second order, symmetric tensors – here $\boldsymbol{E}$ and $\boldsymbol{B}$ – is denoted by ${}^{EB}\widetilde{I}_{1,\ldots,10}$, e.g. ${}^{EB}\widetilde{I}_1 = \boldsymbol{I}{:}\boldsymbol{E}, \ldots, {}^{EB}\widetilde{I}_7 = \boldsymbol{E}{:}\boldsymbol{B}, \ldots,$ ${}^{EB}\widetilde{I}_{10} = [\boldsymbol{E} \cdot \boldsymbol{B} \cdot \boldsymbol{E}]{:}\boldsymbol{B}$, see Appendix A. Obviously the relations ${}^{EB}I_1 = {}^{EB}\widetilde{I}_7$ and ${}^{EB}I_2 = {}^{EB}\widetilde{I}_{10}$ hold (compare Eq. (5)) and furthermore, one easily verifies via the Cayley–Hamilton theorem that ${}^{EB}I_3 = {}^{EB}I_3({}^{EB}\widetilde{I}_{1,\ldots,10})$. Hence, Eq. (5) represents a reduced but physically motivated set of invariants to formulate anisotropic hyper-elasticity or anisotropic inelasticity, respectively.

2.3. Standard dissipative materials

Based on the theory of standard dissipative materials, as introduced by Halphen and Nguyen (1975), the following outline is formulated within the standard reference configuration $\mathscr{B}_0$. Furthermore, an additional internal, scalar-valued hardening variable κ is introduced for completeness and an additive split of the free energy Ψ per unit volume of the form $\Psi = {}^{EB}\Psi(\boldsymbol{E}, \boldsymbol{B}) + {}^{\kappa}\Psi(\kappa)$ is assumed. In view of isothermal processes the dissipation rate density $\mathscr{D}$ per unit volume in $\mathscr{B}_0$ reads

$$\mathscr{D} = \boldsymbol{S} : \dot{\boldsymbol{E}} - \dot{\Psi} = [\boldsymbol{S} - \partial_{\boldsymbol{E}}\Psi] : \dot{\boldsymbol{E}} - \partial_{\boldsymbol{B}}\Psi : \dot{\boldsymbol{B}} - \partial_{\kappa}\Psi \, \dot{\kappa} \geqslant 0. \tag{7}$$

Following the idea that a purely elastic deformation does not produce any dissipation, which means $\boldsymbol{S} - \partial_{\boldsymbol{E}}\Psi \doteq \boldsymbol{0} \; \forall \; \dot{\boldsymbol{E}}$, the hyper-elastic second Piola–Kirchhoff stress tensor $\boldsymbol{S}$, a covariant damage stress tensor $\boldsymbol{\Delta}$ and a scalar-valued hardening stress H are defined via

$$\boldsymbol{S} = \partial_{\boldsymbol{E}}\Psi, \quad \boldsymbol{\Delta} = -\partial_{\boldsymbol{B}}\Psi \quad \text{and} \quad H = \partial_{\kappa}\Psi. \tag{8}$$

Application of these stresses to the Clausius–Duhem inequality (7) results in $\mathscr{D} = \boldsymbol{\Delta}{:}\dot{\boldsymbol{B}} - H\dot{\kappa} \geqslant 0$. Moreover, following the standard scheme, a dissipation surface Φ is introduced which states an admissible elastic domain $\mathbb{A}$ where no damage evolution or hardening takes place

$$\mathbb{A} = \{(\boldsymbol{\Delta}, H) \,|\, \Phi = \Phi(\boldsymbol{\Delta}, H; \boldsymbol{B}) = \varphi(\boldsymbol{\Delta}; \boldsymbol{B}) - Y \leqslant 0\}, \tag{9}$$

with $Y = Y_0 + H(\kappa)$ whereby Y_0 denotes a constant threshold and φ is known as equivalent stress. Next, the postulate of maximum dissipation renders the associated evolution equations

$$\dot{\boldsymbol{B}} = \dot{\gamma}\,\partial_{\boldsymbol{\Delta}}\Phi = \dot{\gamma}\,\partial_{\boldsymbol{\Delta}}\varphi \quad \text{and} \quad \dot{\kappa} = -\dot{\gamma}\,\partial_H\Phi = \dot{\gamma}. \tag{10}$$

Here $\dot{\gamma}$ denotes the Lagrange multiplier and the Kuhn–Tucker conditions completed by the consistency condition read

$$\dot{\gamma} \geqslant 0, \quad \Phi \leqslant 0 \quad \dot{\gamma}\Phi = 0 \quad \text{and} \quad \dot{\gamma}\dot{\Phi} = 0. \tag{11}$$

For convenience the Hessians of the free energy density Ψ are abbreviated by

$${}^{EE}\boldsymbol{\mathscr{L}} = \partial^2_{\boldsymbol{EE}}\Psi, \quad {}^{EB}\boldsymbol{\mathscr{L}} = \partial^2_{\boldsymbol{EB}}\Psi, \quad {}^{BB}\boldsymbol{\mathscr{L}} = \partial^2_{\boldsymbol{BB}}\Psi, \quad {}^{\kappa\kappa}\mathscr{L} = \partial^2_{\kappa\kappa}\Psi, \tag{12}$$

and $[{}^{BE}\boldsymbol{\mathscr{L}}]_{ijkl} = [{}^{EB}\boldsymbol{\mathscr{L}}]_{klij}$, respectively. For notational simplicity two gradients with respect to the dissipation surface Φ are introduced by $\partial_{\boldsymbol{\Delta}}\Phi = \partial_{\boldsymbol{\Delta}}\varphi = \boldsymbol{N}$ and $\partial_{\boldsymbol{B}}\Phi = \partial_{\boldsymbol{B}}\varphi = \boldsymbol{M}$. Furthermore, determining the Lagrange multiplier $\dot{\gamma}$ via the consistency condition in the case of damage evolution or hardening yields

$$\dot{\gamma} = \frac{\boldsymbol{N}:{}^{BE}\boldsymbol{\mathscr{L}}:\dot{\boldsymbol{E}}}{[\boldsymbol{M} - \boldsymbol{N}:{}^{BB}\boldsymbol{\mathscr{L}}]:\boldsymbol{N} - {}^{\kappa\kappa}\mathscr{L}}. \tag{13}$$

Ultimately, the material rates of the hyper-elastic second Piola–Kirchhoff stress tensor $\dot{\boldsymbol{S}}$ and the Green–Lagrange strain tensor $\dot{\boldsymbol{E}}$ are combined by a symmetric fourth order tensor denoted $\boldsymbol{\mathscr{L}}$, in detail

$$\dot{\boldsymbol{S}} = \boldsymbol{\mathscr{L}}:\dot{\boldsymbol{E}} \quad \text{and} \quad \boldsymbol{\mathscr{L}} = {}^{EE}\boldsymbol{\mathscr{L}} - \frac{[{}^{EB}\boldsymbol{\mathscr{L}}:\boldsymbol{N}] \otimes [\boldsymbol{N}:{}^{BE}\boldsymbol{\mathscr{L}}]}{[\boldsymbol{N}:{}^{BB}\boldsymbol{\mathscr{L}} - \boldsymbol{M}]:\boldsymbol{N} + {}^{\kappa\kappa}\mathscr{L}}. \tag{14}$$

Remark 2.2. Note that for the general case where $\bar{\boldsymbol{F}}$ and accordingly $\boldsymbol{B}$ are non-spherical tensors the introduced stresses $\boldsymbol{S}$ and $\boldsymbol{\Delta}$ of Eq. (8) are not coaxial with respect to their conjugate variables $\boldsymbol{E}$ and $\boldsymbol{B}$.

Remark 2.3. Again standard pull-back and push-forward operations applied to the stress tensors render e.g. $\bar{\boldsymbol{S}} = \bar{\boldsymbol{F}}^{-1} \cdot \boldsymbol{S} \cdot \bar{\boldsymbol{F}}^{-\mathrm{T}}$ or $\bar{\boldsymbol{\Delta}} = \bar{\boldsymbol{F}}^{\mathrm{T}} \cdot \boldsymbol{\Delta} \cdot \bar{\boldsymbol{F}}$ – see again Fig. 1. Moreover, the set of invariants due to Eq. (5) define the tensorial stresses of Eq. (8) and straightforward partial differentiation yields

$$\begin{aligned} \boldsymbol{S} &= \Psi_1\,\boldsymbol{B} + 2\,\Psi_2\,\boldsymbol{B}\cdot\boldsymbol{E}\cdot\boldsymbol{B} + 3\,\Psi_3\,\boldsymbol{B}\cdot\boldsymbol{E}\cdot\boldsymbol{B}\cdot\boldsymbol{E}\cdot\boldsymbol{B}, \\ \boldsymbol{\Delta} &= -\Psi_1\,\boldsymbol{E} - 2\,\Psi_2\,\boldsymbol{E}\cdot\boldsymbol{B}\cdot\boldsymbol{E} - 3\,\Psi_3\,\boldsymbol{E}\cdot\boldsymbol{B}\cdot\boldsymbol{E}\cdot\boldsymbol{B}\cdot\boldsymbol{E}, \end{aligned} \tag{15}$$

in connection with the abbreviation $\Psi_i = \partial_{\boldsymbol{EB}\boldsymbol{I}_i}\Psi$.

3. Construction of the evolution equations

This section deals with the construction of rate equations for the internal variables, whereby throughout the hardening stress $H(\kappa)$ and thus Y are assumed to be constant without loss of generality. In the sequel, the existence of a damage potential $\varphi(\boldsymbol{\Delta};\boldsymbol{B})$ within an associated formulation is premised which represents a reduction compared to a general tensor-valued tensor function to compute the rate $\dot{\boldsymbol{B}}$ in terms of the damage stress $\boldsymbol{\Delta}$ and the damage metric $\boldsymbol{B}$, see Appendix B.

A general survey on the construction of rate equations incorporating anisotropy has been given by Betten (1991). For special emphasis on the formulation of plasticity including anisotropic yielding in terms of structural tensors we refer to e.g. Boehler and Sawczuk (1976) or Boehler (1987) for an overview. Anisotropic damage evolution within the small strain case is e.g. treated by Chaboche (1993) or Carol et al. (2001a,b). General surveys on anisotropic damage theory are given by Murakami (1987) or Lemaitre and

Chaboche (1998) among many others. Special emphasis on the evolution of structural tensors in the light of continuum damage mechanics has been pointed out by Matzenmiller and Sackman (1994), Betten et al. (1998) and Menzel and Steinmann (1999).

The general canonical form of the rate equation $\dot{\boldsymbol{B}} = \dot{\boldsymbol{B}}(\boldsymbol{\Delta}; \boldsymbol{B})$ is denoted by

$$\dot{\boldsymbol{B}} = \sum_{\alpha=0}^{2}\sum_{\beta=0}^{2} \phi_{\alpha,\beta}\, {}^{\beta}\boldsymbol{M} : \boldsymbol{\Delta}^{\alpha} \quad \text{with} \quad {}^{\beta}\boldsymbol{M} = \frac{1}{2}\left[\boldsymbol{B}^{\beta} \overline{\otimes} \boldsymbol{I} + \boldsymbol{B}^{\beta} \overline{\otimes} \boldsymbol{I}\right]^{\text{sym}}, \tag{16}$$

see Betten (1992) and Appendix B, respectively. If the existence of a damage potential is assumed, the most general way to introduce this function $\varphi = \varphi(\boldsymbol{\Delta}; \boldsymbol{B})$ is of course based on the set of invariants ${}^{\Delta B}\widetilde{I}_{1,\ldots,10}$ in terms of $\boldsymbol{\Delta}$ and $\boldsymbol{B}$ which renders the associated evolution equation

$$\dot{\boldsymbol{B}} = \dot{\gamma}\, \partial_{\boldsymbol{\Delta}} \varphi = \dot{\gamma} \sum_{i=1,2,3,7}^{10} \partial_{{}^{\Delta B}\widetilde{I}_i} \varphi\, \partial_{\boldsymbol{\Delta}}\, {}^{\Delta B}\widetilde{I}_i \quad \text{with} \quad \varphi = \varphi({}^{\Delta B}\widetilde{I}_{1,\ldots,10}). \tag{17}$$

Nevertheless, this rather general potential approach represents a restricted form of the general canonical equation (16), compare Appendix B.

On the other side, two selected representations of Eq. (17) seem to be natural, see e.g. Schreyer (1995):

The direct formulation is actually based on a second order, positive semi-definite tensor ${}^{2}\boldsymbol{\Xi}$ which directly defines the evolution equation $\dot{\boldsymbol{B}} = -\dot{\gamma}^2 \boldsymbol{\Xi}$. This is one to one with $\varphi = -{}^{2}\boldsymbol{\Xi} : \boldsymbol{\Delta}$ and a straightforward calculation using the loading conditions $\Phi \leqslant 0$ and $\dot{\gamma} \geqslant 0$ yields the dissipation inequality $\mathscr{D} = \dot{\gamma} Y \geqslant 0$.

The formulation based on conjugate variables constitutes the damage rate via a linear map of the damage stress, in detail $\dot{\boldsymbol{B}} = \dot{\gamma}\, {}^{4}\boldsymbol{\Xi} : \boldsymbol{\Delta}$ whereby ${}^{4}\boldsymbol{\Xi}$ is some positive semi-definite, fourth order tensor. The corresponding damage function reads $\varphi = 1/2 \boldsymbol{\Delta} : {}^{4}\boldsymbol{\Xi} : \boldsymbol{\Delta}$ which renders a Clausius–Duhem inequality of the form $\mathscr{D} = 2\dot{\gamma} Y \geqslant 0$.

As a first example the simplest case of a direct formulation is considered by ${}^{2}\boldsymbol{\Xi} \doteq \boldsymbol{B}$ which ends up in

$$\varphi_1 = -\boldsymbol{B} : \boldsymbol{\Delta} \quad \text{and} \quad \dot{\boldsymbol{B}} = -\dot{\gamma} \boldsymbol{B}. \tag{18}$$

Although the damage metric is just scaled down in the case of damage evolution this approach differs significantly from the standard isotropic [1-D] continuum damage formulation since $\boldsymbol{B}$ is not necessarily a spherical tensor which renders a generally overall anisotropic material behavior. Nevertheless, in the light that the damage rate $\dot{\boldsymbol{B}}$ is throughout coaxial to the damage metric $\boldsymbol{B}$ itself, Eq. (18) will be referred to as quasi-isotropic damage.

Contrary, the damage evolution is identified as truly anisotropic if $\dot{\boldsymbol{B}}$ and $\boldsymbol{B}$ are generally not coaxial. The rotation of the principle damage directions is generally guaranteed e.g. by ${}^{4}\boldsymbol{\Xi} = \boldsymbol{B} \overline{\otimes} \boldsymbol{B}$, see Appendix A for the definition of the non-standard dyadic product $\overline{\otimes}$. Now, the damage function and rate equation read

$$\varphi_2 = \tfrac{1}{2} \boldsymbol{\Delta} : [\boldsymbol{B} \overline{\otimes} \boldsymbol{B}] : \boldsymbol{\Delta} \quad \text{and} \quad \dot{\boldsymbol{B}} = \dot{\gamma} [\boldsymbol{B} \overline{\otimes} \boldsymbol{B}] : \boldsymbol{\Delta}, \tag{19}$$

which has formally the structure of a base transformation $\dot{\boldsymbol{B}} = \dot{\gamma} \boldsymbol{B} \cdot \boldsymbol{\Delta} \cdot \boldsymbol{B}^{\mathrm{T}}$.

Remark 3.1. Note again that standard isotropic damage is included in the proposed framework for $\bar{\boldsymbol{F}} \doteq \beta_0 \boldsymbol{I}$ coupled to quasi-isotropic damage.

Remark 3.2. Adopting the structure of the standard second and fourth order identity tensors within the construction of the proposed damage functions yields

$${}^{2}\boldsymbol{\Xi} = {}^{2}\eta \boldsymbol{B} \quad \text{and} \quad {}^{4}\boldsymbol{\Xi} = {}^{4}\eta_1 \boldsymbol{B} \otimes \boldsymbol{B} + {}^{4}\eta_2 [\boldsymbol{B} \overline{\otimes} \boldsymbol{B} + \boldsymbol{B} \underline{\otimes} \boldsymbol{B}], \tag{20}$$

whereby due to the central idea of the whole formulation the second order identity tensor $\bar{\boldsymbol{I}} \doteq \bar{\boldsymbol{B}} \in \bar{\mathscr{B}}_0$ was replaced by the damage metric $\boldsymbol{B} \in \mathscr{B}_0$ to end up with anisotropic formulations in the standard reference

configuration, compare Betten (1988). Moreover, for a non-spherical tensor $\boldsymbol{B}$ the second part of Eq. (20) constitutes anisotropic damage evolution in the sense that the principle damage directions ${}^{B}\boldsymbol{n}$ do not stay constant during the damage process which means $\dot{\boldsymbol{B}}$ and $\boldsymbol{B}$ are not coaxial tensors. Furthermore, the standard dyadic product renders a contribution within the category of quasi-isotropic damage and due to the fact that both $\boldsymbol{\Delta}$ and $\boldsymbol{B}$ are symmetric the two non-standard dyadic products end up in identical terms for the damage rate $\dot{\boldsymbol{B}}$. This motivates the chosen damage function of Eq. (19).

Remark 3.3. With these two damage functions φ_1 and φ_2 of Eqs. (18) and (19) in hand a general classification of the coupling of hyper-elasticity and damage is possible which renders the following four categories

1. isotropic hyper-elasticity ($\boldsymbol{B}_0 = \alpha_0 \boldsymbol{I}$) and quasi-isotropic damage (φ_1),
2. isotropic hyper-elasticity ($\boldsymbol{B}_0 = \alpha_0 \boldsymbol{I}$) and anisotropic damage (φ_2),
3. anisotropic hyper-elasticity ($\boldsymbol{B}_0 \neq \alpha_0 \boldsymbol{I}$) and quasi-isotropic damage (φ_1),
4. anisotropic hyper-elasticity ($\boldsymbol{B}_0 \neq \alpha_0 \boldsymbol{I}$) and anisotropic damage (φ_2),

whereby $\boldsymbol{B}_0 \in \mathscr{B}_0$ denotes the initial damage metric. Note that formulations within category 2 become generally anisotropic within the elastic domain in the case of unloading after damage evolution has taken place.

4. Numerical time integration

A fundamental part of any formulation on continuum damage mechanics or elasto-plasticity is the numerical (time-) integration of the corresponding rate equations. Usually, families of radial-return algorithms are applied, see e.g. Simo (1998) for an overview with respect to plasticity. Based on the rate-independent framework given in Section 2 a staggered algorithmic treatment is applied. Thus, from the computational point of view, the classical time interval of interest $\mathbb{T} = \bigcup_{n=0}^{N} [{}^{n}t, {}^{n+1}t]$ is actually discretized into n time steps which define a strain driven algorithm. Please note that for the highlighted Algorithms 1–3 loading and unloading is exclusively checked by the trial step at ${}^{n+1}\boldsymbol{E}$.

To set the stage quasi-isotropic damage is considered first. Since the principle directions of the damage metric $\boldsymbol{B}$ stay constant during the damage process an exponential scheme can be applied, compare Weber and Anand (1990, Eq. (26)). Within the example of Eq. (18) the algorithm reduces to a scalar-valued iteration, Algorithm 1.

Algorithm 1. Exponential integration algorithm for quasi-isotropic damage, Eq. (18).

if $\Phi(\boldsymbol{\Delta}({}^{n+1}\boldsymbol{E}, {}^{n}\boldsymbol{B}), {}^{n}\boldsymbol{B}) > 0$
dowhile $|\Phi(\Delta\gamma, \boldsymbol{\Delta}({}^{n+1}\boldsymbol{E}, {}^{n+1}\boldsymbol{B}), {}^{n+1}\boldsymbol{B})| > \mathrm{tol}$
$\quad {}^{n+1}\boldsymbol{B} = \exp(-\Delta\gamma)\, {}^{n}\boldsymbol{B}$
enddo

Several families of algorithms to solve for the roots of non-linear scalar-valued equations exist, see e.g. Engeln-Müllges and Uhlig (1996) for a detailed outline. Within our numerical computations we prefer a modified Regula-Falsi scheme due to Anderson and Björck which results in a much more stable algorithm than interpolation or Newton's methods.

For the general anisotropic case due to Eq. (19) several algorithms of the Runge–Kutta family can be applied for the integration of the system of ordinary differential equations (initial value problem), see the textbooks by Lambert (1991), Ascher and Petzold (1998) among many others for a general, mathematical

overview and e.g. Hackl (1998), Diebels et al. (1998) and Kirchner and Kollmann (1999) with respect to the integration of rate equations in the context of higher order Runge–Kutta schemes.

In the sequel, we restrict to implicit integrations. Obviously, explicit schemes are included in the outline but lead again to scalar-valued iterations with respect to the Lagrange multipliers. Generally Runge–Kutta methods are defined by the (s-stage) Butcher array

$$\begin{array}{c|cccc} c_1 & a_{11} & a_{12} & \cdots & a_{1s} \\ c_2 & a_{21} & a_{22} & \cdots & a_{2s} \\ \vdots & \vdots & \vdots & \ddots & \vdots \\ c_s & a_{s1} & a_{s2} & \cdots & a_{ss} \\ \hline & b_1 & b_2 & \cdots & b_s \end{array}$$

whereby without loss of generality $\sum_{i=1}^{s} b_i = 1$ and $c_i = \sum_{j}^{s} a_{ij}$ are assumed, see Appendix C for a small collection of examples. Hence, for higher order methods several intermediate stages $\boldsymbol{B}_i$ are implicitly defined by

$$\boldsymbol{B}_i = {}^{n}\boldsymbol{B} + \Delta\gamma_i \sum_{j=1}^{s} a_{ij}\, \partial_{\boldsymbol{\Delta}_j} \Phi({}^{n+c_j}\boldsymbol{E}, \boldsymbol{B}_j) \tag{21}$$

and the actual damage metric ${}^{n+1}\boldsymbol{B}$ is computed via

$${}^{n+1}\boldsymbol{B} = {}^{n}\boldsymbol{B} + \Delta\gamma \sum_{i=1}^{s} b_i\, \partial_{\boldsymbol{\Delta}_i} \Phi({}^{n+c_i}\boldsymbol{E}, \boldsymbol{B}_i), \tag{22}$$

whereby for simplicity the notation $\boldsymbol{\Delta}_i = \boldsymbol{\Delta}({}^{n+c_i}\boldsymbol{E}, \boldsymbol{B}_i)$ was adopted. These non-linear equations are solved for given $\Delta\gamma_i$ by a local Newton algorithm which yields within each iteration k the linear system of equations

$$\begin{bmatrix} \mathbf{1}^{\mathrm{sym}} - \Delta\gamma_1 a_{11} \boldsymbol{J}_1 & -\Delta\gamma_1 a_{12} \boldsymbol{J}_2 & \cdots \\ -\Delta\gamma_2 a_{21} \boldsymbol{J}_1 & \mathbf{1}^{\mathrm{sym}} - \Delta\gamma_2 a_{22} \boldsymbol{J}_2 & \cdots \\ \vdots & \vdots & \ddots \\ -\Delta\gamma_s a_{s1} \boldsymbol{J}_1 & -\Delta\gamma_s a_{s2} \boldsymbol{J}_2 & \cdots \end{bmatrix} \begin{bmatrix} \Delta\boldsymbol{B}_1 \\ \Delta\boldsymbol{B}_1 \\ \vdots \\ \Delta\boldsymbol{B}_s \end{bmatrix} = - \begin{bmatrix} \boldsymbol{R}_1 \\ \boldsymbol{R}_1 \\ \vdots \\ \boldsymbol{R}_s \end{bmatrix}, \tag{23}$$

together with the residuum $\boldsymbol{R}_i = {}_{k}\boldsymbol{B}_i - {}^{n}\boldsymbol{B} - \Delta\gamma_i \sum_{j=1}^{s} a_{ij}\, \partial_{\boldsymbol{\Delta}_j} \Phi({}^{n+c_j}\boldsymbol{E}, {}_{k}\boldsymbol{B}_j)$, the Jacobians $\boldsymbol{J}_i = \partial^2_{\boldsymbol{\Delta}_i\, {}_{k}\boldsymbol{B}_i} \times \Phi({}^{n+c_i}\boldsymbol{E}, {}_{k}\boldsymbol{B}_i)$ and the update ${}_{k+1}\boldsymbol{B}_i = {}_{k}\boldsymbol{B}_i + \Delta\boldsymbol{B}_i$.

Remark 4.1. Voigt's notation is used to solve the system (23) and symmetry yields $\Delta\boldsymbol{B}_i$, $\boldsymbol{R}_i \in \mathbb{R}^6$ and consequently $\mathbf{1}^{\mathrm{sym}}$, $\boldsymbol{J}_i \in \mathbb{R}^6 \times \mathbb{R}^6$.

Remark 4.2. In view of Eq. (19) the Jacobians are defined by

$$\begin{aligned} \boldsymbol{J}_i &= \partial_{{}_{k}\boldsymbol{B}_i}([{}_{k}\boldsymbol{B}_i \overline{\otimes}\, {}_{k}\boldsymbol{B}_i]{:}\boldsymbol{\Delta}_i) \\ &= [\partial_{{}_{k}\boldsymbol{B}_i}({}_{k}\boldsymbol{B}_i \overline{\otimes}\, {}_{k}\boldsymbol{B}_i)]{:}\boldsymbol{\Delta}_i - [{}_{k}\boldsymbol{B}_i \overline{\otimes}\, {}_{k}\boldsymbol{B}_i]{:}^{BB}\boldsymbol{\mathscr{L}}_i. \end{aligned} \tag{24}$$

Accomplishing the differentiation of the first term yields in index notation with respect to a Cartesian frame $\left[1^{\mathrm{sym}}_{imkl} B_{jn} + B_{im} 1^{\mathrm{sym}}_{jnkl}\right]{:}\boldsymbol{\Delta}_{mn}$. Moreover, the Hessian ${}^{BB}\boldsymbol{\mathscr{L}} = -\partial_{\boldsymbol{B}}\boldsymbol{\Delta}$ in terms of invariants (see Eqs. (5) and (15)) using the abbreviations $\Psi_i = \partial_{{}^{EB}I_i}\Psi$ and $\Psi_{ij} = \partial^2_{{}^{EB}I_i\, {}^{EB}I_j}\Psi$ reads

$$
\begin{aligned}
{}^{BB}\mathscr{L} = {} & \Psi_{11}\boldsymbol{E}\otimes\boldsymbol{E} + 4\Psi_{22}[\boldsymbol{E}\cdot\boldsymbol{B}\cdot\boldsymbol{E}]\otimes[\boldsymbol{E}\cdot\boldsymbol{B}\cdot\boldsymbol{E}] + 9\Psi_{33}[\boldsymbol{E}\cdot\boldsymbol{B}\cdot\boldsymbol{E}\cdot\boldsymbol{B}\cdot\boldsymbol{E}]\otimes[\boldsymbol{E}\cdot\boldsymbol{B}\cdot\boldsymbol{E}\cdot\boldsymbol{B}\cdot\boldsymbol{E}] \\
& + 2\Psi_{12}\Big[[\boldsymbol{E}\cdot\boldsymbol{B}\cdot\boldsymbol{E}]\otimes\boldsymbol{E} + \boldsymbol{E}\otimes[\boldsymbol{E}\cdot\boldsymbol{B}\cdot\boldsymbol{E}]\Big] \\
& + 3\Psi_{13}\Big[[\boldsymbol{E}\cdot\boldsymbol{B}\cdot\boldsymbol{E}\cdot\boldsymbol{B}\cdot\boldsymbol{E}]\otimes\boldsymbol{E} + \boldsymbol{E}\otimes[\boldsymbol{E}\cdot\boldsymbol{B}\cdot\boldsymbol{E}\cdot\boldsymbol{B}\cdot\boldsymbol{E}]\Big] \\
& + 6\Psi_{23}\Big[[\boldsymbol{E}\cdot\boldsymbol{B}\cdot\boldsymbol{E}\cdot\boldsymbol{B}\cdot\boldsymbol{E}]\otimes[\boldsymbol{E}\cdot\boldsymbol{B}\cdot\boldsymbol{E}] + [\boldsymbol{E}\cdot\boldsymbol{B}\cdot\boldsymbol{E}]\otimes[\boldsymbol{E}\cdot\boldsymbol{B}\cdot\boldsymbol{E}\cdot\boldsymbol{B}\cdot\boldsymbol{E}]\Big] \\
& + 2\Psi_2{}^{EBE}\boldsymbol{\Xi}_B + 3\Psi_3{}^{EBEBE}\boldsymbol{\Xi}_B,
\end{aligned}
\tag{25}
$$

with $[{}^{EBEBE}\boldsymbol{\Xi}_B]_{ijkl} = E_{im}E_{no}E_{pj}\Big[1^{\mathrm{sym}}_{mnkl}B_{op} + B_{mn}1^{\mathrm{sym}}_{opkl}\Big]$ and $[{}^{EBE}\boldsymbol{\Xi}_B]_{ijkl} = E_{im}E_{nj}1^{\mathrm{sym}}_{mnkl}$ in index notation with respect to a cartesian frame, respectively.

In view of a staggered formulation, i.e. the Newton iteration for the damage metric is embedded into scalar-valued iterations to compute the Lagrange multiplier, two schemes are possible. Within the first algorithm the intermediate stages $\boldsymbol{B}_i$ are not forced to fulfil the damage condition and $\Phi(\boldsymbol{\Delta}_i, \boldsymbol{B}_i) > 0$ is possible. Since solely the actual configuration has to lie in the elastic domain $\mathbb{A}$, requiring $\Phi({}^{n+1}\boldsymbol{\Delta}, {}^{n+1}\boldsymbol{B}) = 0$, this scheme ends up in only one damage multiplier, Algorithm 2.

Algorithm 2. Integration Scheme 1: Intermediate stages are not forced to fulfil the damage condition.

if $\Phi(\boldsymbol{\Delta}({}^{n+1}\boldsymbol{E}, {}^{n}\boldsymbol{B}), {}^{n}\boldsymbol{B}) > 0$
dowhile $|\Phi(\Delta\gamma, \boldsymbol{\Delta}({}^{n+1}\boldsymbol{E}, {}^{n+1}\boldsymbol{B}), {}^{n+1}\boldsymbol{B})| > \mathrm{tol}$
  dowhile $\|\Delta\boldsymbol{B}_i\| > \mathrm{tol}$
    $\boldsymbol{B}_i = {}^{n}\boldsymbol{B} + \Delta\gamma\sum_{j=1}^{s} a_{ij}\,\partial_{\boldsymbol{\Delta}_j}\Phi({}^{n+c_j}\boldsymbol{E}, \boldsymbol{B}_j)$
  enddo
  ${}^{n+1}\boldsymbol{B} = {}^{n}\boldsymbol{B} + \Delta\gamma\sum_{i=1}^{s} \boldsymbol{b}_i\,\partial_{\boldsymbol{\Delta}_i}\Phi({}^{n+c_i}\boldsymbol{E}, \boldsymbol{B}_i)$
enddo

Alternatively, the second integration category forces the intermediate stages to satisfy the damage condition. Now, all stages of interest lie in the elastic domain $\mathbb{A}$ but from the numerical point of view several scalar-valued iterations for different Lagrange multipliers due to each intermediate stage come into the picture. Furthermore, if the considered interval includes damaged and purely elastic regions as well, the rate equation is not smooth anymore which may cause numerical instabilities for large integration intervals.

Algorithm 3. Integration Scheme 2: Intermediate stages are forced to fulfil the damage condition.

if $\Phi(\boldsymbol{\Delta}({}^{n+1}\boldsymbol{E}, {}^{n}\boldsymbol{B}), {}^{n}\boldsymbol{B}) > 0$
if $\Phi(\boldsymbol{\Delta}({}^{n+c_i}\boldsymbol{E}, {}^{n}\boldsymbol{B}), {}^{n}\boldsymbol{B}) > 0$
dowhile $|\Phi(\Delta\gamma_i, \boldsymbol{\Delta}_i, \boldsymbol{B}_i)| > \mathrm{tol}$
  dowhile $||\Delta\boldsymbol{B}_i|| > \mathrm{tol}$
    $\boldsymbol{B}_i = {}^{n}\boldsymbol{B} + \Delta\gamma_i\sum_{j=1}^{s} a_{ij}\,\partial_{\boldsymbol{\Delta}_j}\Phi({}^{n+c_j}\boldsymbol{E}, \boldsymbol{B}_j)$
  enddo
enddo
dowhile $|\Phi(\Delta\gamma, \boldsymbol{\Delta}({}^{n+1}\boldsymbol{E}, {}^{n+1}\boldsymbol{B}), {}^{n+1}\boldsymbol{B})| > \mathrm{tol}$
  ${}^{n+1}\boldsymbol{B} = {}^{n}\boldsymbol{B} + \Delta\gamma\sum_{i=1}^{s} b_i\,\partial_{\boldsymbol{\Delta}_i}\Phi({}^{n+c_i}\boldsymbol{E}, \boldsymbol{B}_i)$
enddo

Remark 4.3. Note that both Algorithms 2 and 3 are identical in the case of an Euler backward integration.

Remark 4.4. As usual, the intermediate strain metrics are defined by linear interpolation ${}^{n+c_i}\boldsymbol{E} = c_i {}^{n+1}\boldsymbol{E} + [1-c_i]{}^{n}\boldsymbol{E}$. Moreover, it is useful to choose as an initial guess (ini) within diagonally implicit Runge–Kutta schemes $\boldsymbol{B}_j^{\text{ini}} := \boldsymbol{B}_i$ for $c_j > c_i$ instead of the standard initialization $\boldsymbol{B}_i^{\text{ini}} := {}^{n}\boldsymbol{B}$.

5. Numerical examples

To discuss overall anisotropic behavior within the proposed framework of coupling hyper-elasticity to continuum damage the homogeneous deformation of simple shear is considered. Both types of damage evolution due to Eqs. (18) and (19) are outlined. Furthermore, we directly start with anisotropic hyper-elasticity which yields examples within categories 3 and 4 of Remark 3.3.

The overall definition of anisotropy is given by the non-coaxiality of stress and strain which means that the unsymmetric part of their product does not vanish. Hence, for the general case of anisotropic damage evolution in the spirit of the proposed framework, the relations

$$\boldsymbol{S}\cdot\boldsymbol{E}-\boldsymbol{E}\cdot\boldsymbol{S}\neq\boldsymbol{0} \quad \text{and} \quad \boldsymbol{B}_0\cdot\boldsymbol{B}-\boldsymbol{B}\cdot\boldsymbol{B}_0\neq\boldsymbol{0} \quad \text{in} \quad \mathscr{B}_0 \tag{26}$$

generally hold, whereby $\boldsymbol{B}_0$ denotes the initial damage metric. To visualize this non-coaxiality the method of stereo-graphic projection is applied, which is well known from crystallography representing a homomorphism $SO(3) \to SU(2)$, see e.g. Altmann (1986, Chapter 7). Clearly, the eigenvectors of symmetric, second order tensors (which are themselves part of the unit sphere S^2) are projected onto the equatorial plane by viewing from the south pole, see Fig. 2(a).

Furthermore, to define the initial eigenvectors $\boldsymbol{n}_I$ of the damage metric due to Eq. (6) spherical coordinates with respect to a cartesian frame $\boldsymbol{e}_i$ are applied, see Fig. 2(b); namely, $\boldsymbol{n}_I = n_I^i \boldsymbol{e}_i$ with $n_I^1 = \sin\vartheta_I^1 \sin\vartheta_I^2$, $n_I^2 = \cos\vartheta_I^2$, $n_I^1 = \cos\vartheta_I^1 \sin\vartheta_I^2$ and $I = 1,2$ in view of Eq. (6).

Within the hyper-elastic context coupled to continuum damage mechanics a compressible Mooney–Rivlin material is considered, to be specific

$${}^{\bar{C}\bar{B}}\bar{\Psi}(\bar{\boldsymbol{C}},\bar{\boldsymbol{B}}) = c_1[{}^{\bar{C}}J_1 - 3] + c_2[{}^{\bar{C}}J_2 - 3] + \frac{1}{2}\lambda^{\mathrm{p}} \ln^2\left(\sqrt{{}^{\bar{C}}J_3}\right) - 2[c_1 + 2c_2]\ln\left(\sqrt{{}^{\bar{C}}J_3}\right) \tag{27}$$

in terms of the effective right Cauchy–Green tensor $\bar{\boldsymbol{C}}$ together with $\bar{\boldsymbol{B}} \doteq \bar{\boldsymbol{I}}$. The anisotropic damage formulation is defined by replacing the invariants ${}^{\bar{C}}J_i$ by the set ${}^{EB}I_i$ as given in Eq. (A.7) in Appendix A, skipping some trivial but tedious details on differentiation due to the stresses and Hessians.

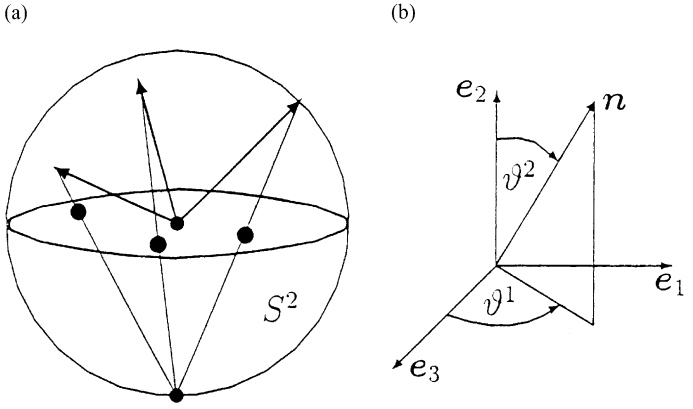

Fig. 2. (a) Stereo-graphic projection and (b) spherical coordinates.

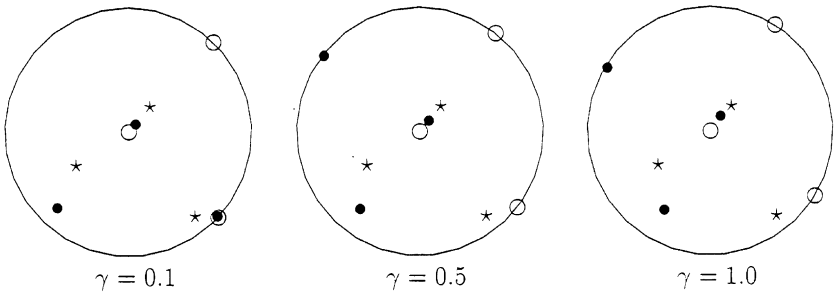

Fig. 3. Simple shear, quasi-isotropic damage: stereo-graphic projection due to the principle directions of strain $\boldsymbol{E}(\bigcirc)$, stress $\boldsymbol{S}(\bullet)$ and the damage metric $\boldsymbol{B}(\bigstar)$.

Within the considered homogeneous deformation of simple shear ($\boldsymbol{F} = \boldsymbol{I} + \gamma \boldsymbol{e}_1 \otimes \boldsymbol{e}_2 \rightarrow {}^E\boldsymbol{n}_I \neq \text{const}$) anisotropic hyper-elasticity coupled to quasi-isotropic and anisotropic damage is pointed out. Thereby, the parameters of the compressible Mooney–Rivlin material given in Eq. (27) read $c_1 = 10$, $c_2 = 20$ and $\lambda^{\mathrm{p}} = 5$. A constant threshold $Y = 10$ is chosen and the initial damage metric $\boldsymbol{B}_0$ is defined by $\alpha_0 = 1$, $\alpha_1 = 1/2$, $\alpha_2 = 1/4$, $\vartheta_1^1 = (2/3)\pi$, $\vartheta_1^2 = (1/3)\pi$, $\vartheta_2^1 = (4/3)\pi$ and $\vartheta_2^2 = (1/6)\pi$ – see Eq. (6) and Fig. 2(b). With slight danger of confusion the shear parameter will be denoted by γ.

5.1. Quasi-isotropic damage

In the sequel quasi-isotropic damage evolution due to the potential φ_1 of Eq. (18) is applied which ends up together with the non-spherical $\boldsymbol{B}_0$ in a damage formulation within category 3 of Remark 3.3. Thus, stress $\boldsymbol{S}$ and strain $\boldsymbol{E}$ do not have identical principle directions but the eigenvectors of the damage metric $\boldsymbol{B}$ stay constant for arbitrary deformations. Fig. 3 visualizes these effects by the method of stereo-graphic projection for $\gamma = 0.1, 0.5, 1.0$.

Concerning the numerical integration of the obtained rate equation of $\dot{\boldsymbol{B}}$ (Eq. (18)) the exponential scheme given in Algorithm 1 is applied. Finally, the corresponding degradation of the eigenvalues ${}^B\lambda_I$ due to the damage metric are depicted in Fig. 4.

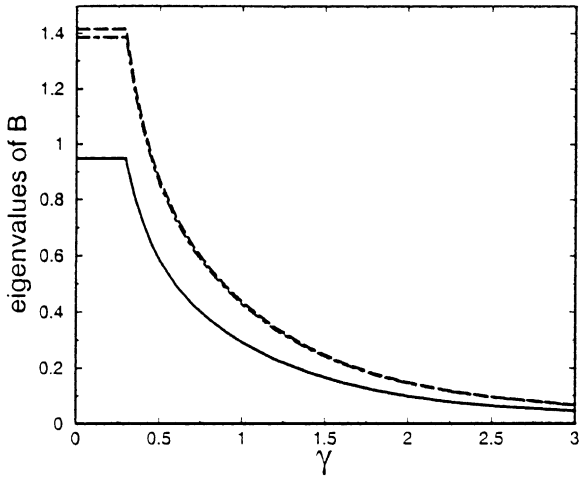

Fig. 4. Simple shear, quasi-isotropic damage: degradation of the eigenvalues ${}^B\lambda_I$.

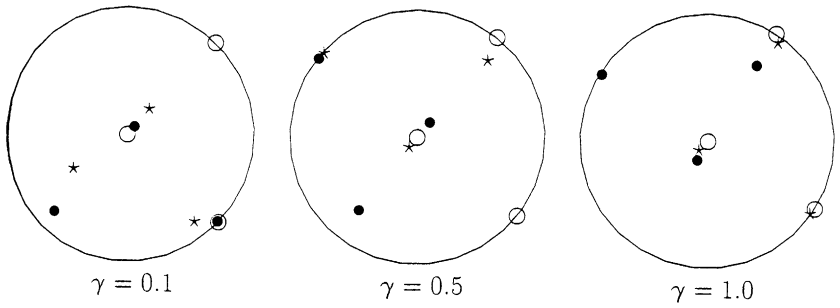

Fig. 5. Simple shear, anisotropic damage: stereo-graphic projection due to the principle directions of strain $\boldsymbol{E}(\bigcirc)$, stress $\boldsymbol{S}(\bullet)$ and the damage metric $\boldsymbol{B}(\bigstar)$.

5.2. Anisotropic damage

Next, anisotropic damage evolution due to the potential φ_2 of Eq. (19) within the same setting as above is applied. This together with the non-spherical initial damage metric $\boldsymbol{B}_0$ results in a damage formulation within category 4 of Remark 3.3. Thus, stress $\boldsymbol{S}$ and strain $\boldsymbol{E}$ do generally not have identical principle directions and additionally the damage metric $\boldsymbol{B}_0$ and $\boldsymbol{B}$ are not coaxial anymore if damage evolution takes place. Making again use of the method of stereo-graphic projection allows to give a graphical representation of these general anisotropic characteristics, see Fig. 5 for deformations one to one with $\gamma = 0.1, 0.5, 1.0$.

Due to the fact that the eigenvectors of the initial damage metric ${}^{B_0}\boldsymbol{n}_I$ have contributions in all three directions $\boldsymbol{e}_i$ and that additionally the anisotropic damage function φ_2 is applied all three eigenvalues of the damage metric ${}^{B}\lambda_I$ degrade differently, see Fig. 6 (the reference solution has been computed within a fourth order Runge–Kutta scheme for load steps $h{:}\Delta\gamma = 0.02$).

Now, explicit Runge–Kutta schemes of order one up to four are applied for the integration of the rate equation of $\dot{\boldsymbol{B}}$, Eq. (19). Because of stability reasons, the load steps h – actually in terms of strains – have to be chosen so small (here e.g. $h{:}\Delta\gamma = 0.1$) that the accuracy of the integration scheme is not significant

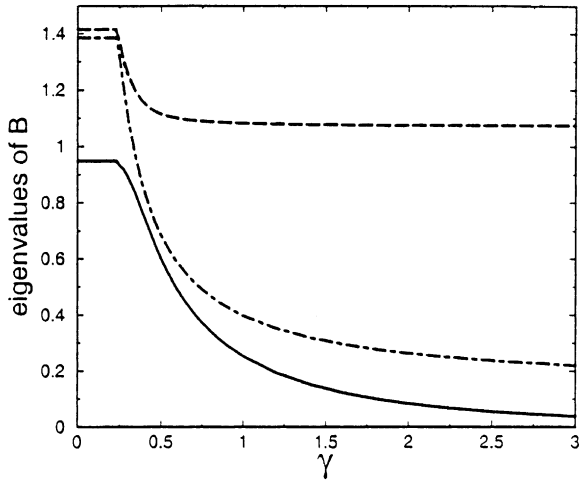

Fig. 6. Simple shear, anisotropic damage: degradation of the eigenvalues ${}^{B}\lambda_I$.

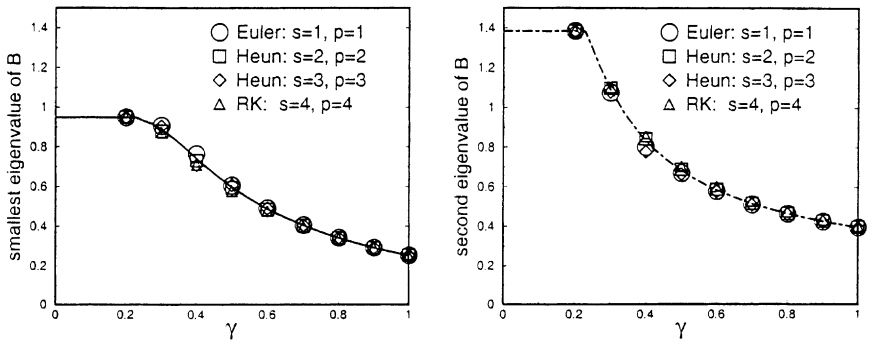

Fig. 7. Simple shear, anisotropic damage: degradation of the smallest and second eigenvalue ${}^{B}\lambda_I$ of the damage metric within explicit integration algorithms due to Scheme 2.

anymore as depicted in Fig. 7 for the smallest and second eigenvalue of $\boldsymbol{B}$. Although at $\gamma = 0.4$ the considered integration algorithms render somewhat different results they end up in identical eigenvalues ${}^{B}\lambda_I$ for increasing damage as far as the eye can catch. Furthermore, integration Scheme 2 was applied (see Algorithm 3) which is not significant for such small load steps.

Next, a large integration interval starting in the elastic area and ending up in the damaged domain is considered $(h{:}[\gamma = 0.1, \gamma = 1.0])$. Thereby implicit Runge–Kutta schemes within category 1 and 2 are applied (see Algorithms 2 and 3). Remember that the intermediate stages are forced to fulfil the damage condition within category 2 and otherwise not, respectively. Again algorithms of order one up to four are analyzed, see Appendix C for some details.

Fig. 8(a)–(d) visualize the numerical results again for the smallest and second eigenvalue of the damage metric with respect to integration Scheme 1. Now, within this large interval of loading, the numerical results for different integration algorithms differ significantly, especially for the smallest eigenvalue of the damage metric. Within Scheme 1 (Algorithm 2 diagonally implicit Runge–Kutta schemes (DIRK) – Fig. 8(c) and (d) – show similar upshots as standard Runge–Kutta schemes – Fig. 8(a) and (b). On the other hand, integration Scheme 2 due to Algorithm 3 forces the intermediate stages to satisfy the damage condition. As depicted in Fig. 8(e) and (f) the numerical results obtained by DIRK methods become more accurate.

Next, an integration interval is considered which lies completely in the damage domain $(h{:}[\gamma = 0.25, \gamma = 1.0])$. Similar to Fig. 8 the corresponding numerical results are depicted in Fig. 9. Since the integration interval is now smaller compared to the above example and in addition the corresponding function is smooth, all numerical results become more accurate. Nevertheless, especially the standard implicit Runge–Kutta algorithms within Scheme 1 (Fig. 9(a) and (b)) render different eigenvalues and again DIRK methods within Scheme 2 (Fig. 9(e) and (f)) end up with the most accurate computations.

Remark 5.1. Obviously, integration algorithms within Scheme 2 require several scalar-valued iterations to compute all Lagrange multipliers. Nevertheless, the overall numerical costs are in general not necessarily higher than applying category 1 since each iteration reaches faster convergence compared to the single one within integration Scheme 1. Apparently, category 2 behaves numerically more stable than category 1 as far as large integration intervals for a sufficiently smooth function are considered.

6. Summary and conclusions

The main goal of this contribution has been the formulation of a large strain continuum damage framework taking overall anisotropy based on second order metrics into account. Thereby, the developed

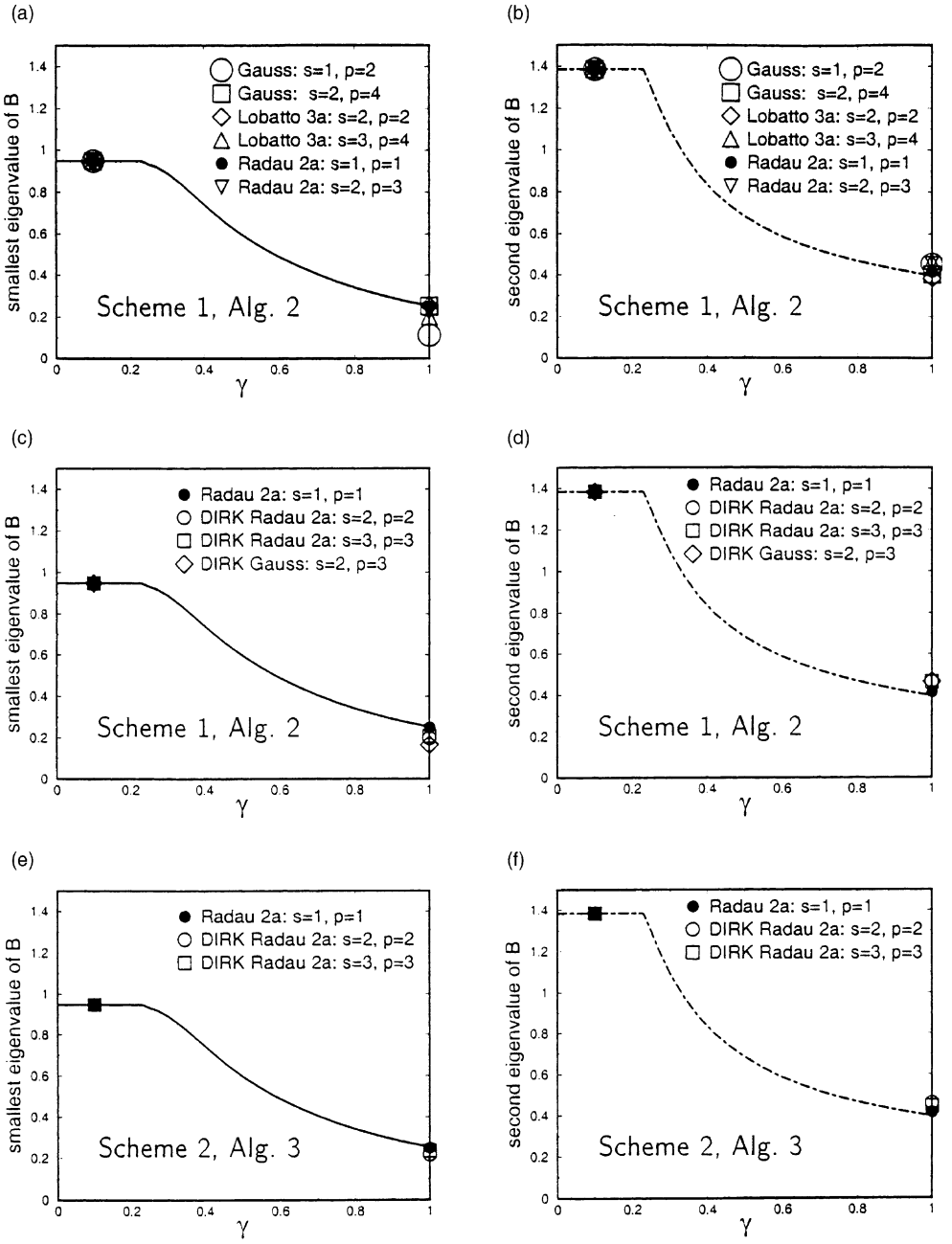

Fig. 8. Simple shear, anisotropic damage: degradation of the smallest and second eigenvalue ${}^{B}\lambda_I$ of the damage metric within implicit integration algorithms due to an elastic-damage interval.

theory is straightforwardly based on the concept of strain energy equivalence between a fictitious, undamaged, isotropic and a damaged, anisotropic reference configuration as proposed in Steinmann and Carol (1998).

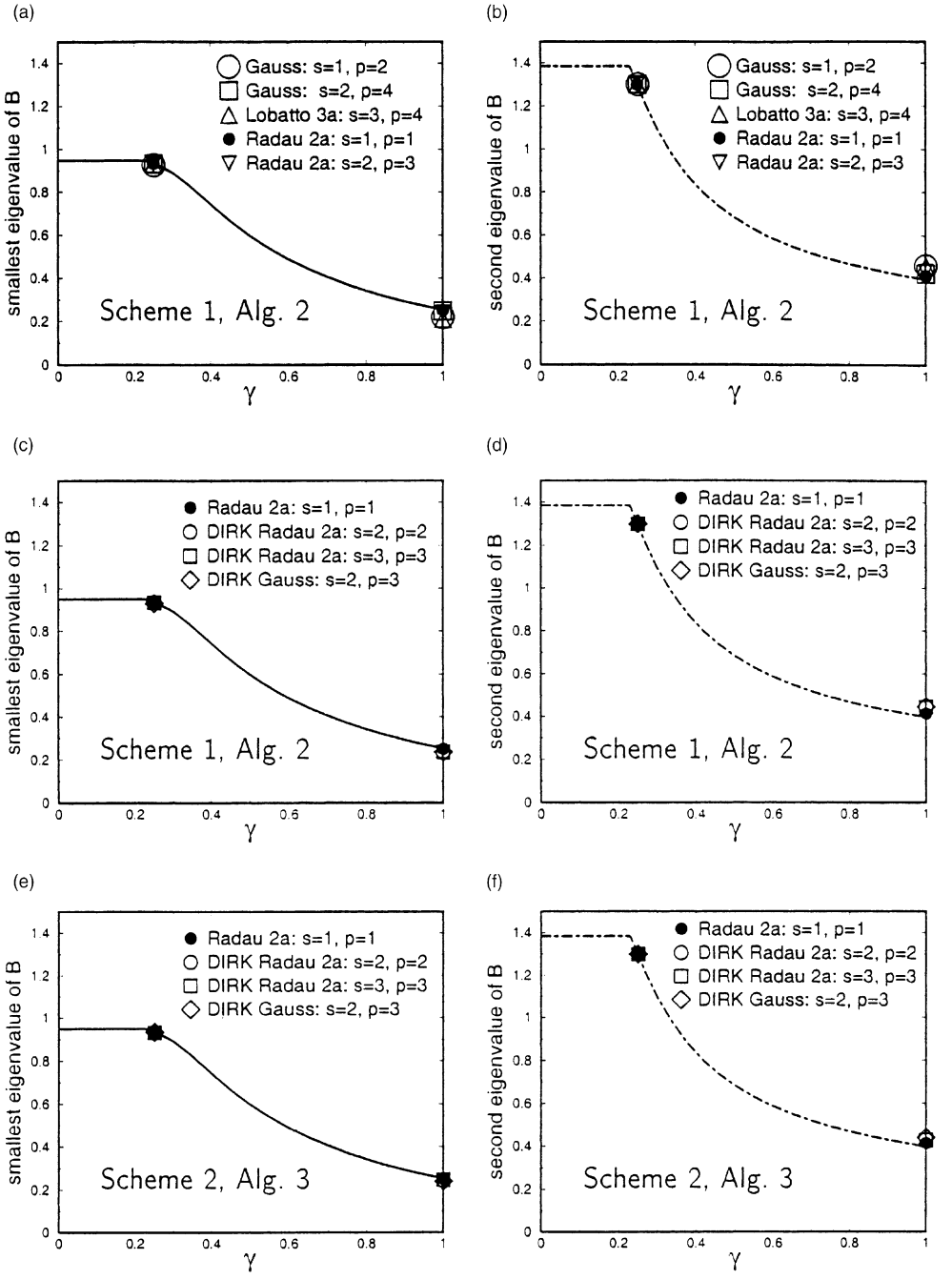

Fig. 9. Simple shear, anisotropic damage: degradation of the smallest and second eigenvalue ${}^{B}\lambda_I$ of the damage metric within implicit integration algorithms due to an damage–damage interval.

A general, second order, large strain continuum damage formulation in terms of two second order, symmetric tensors ends up with a set of 10 invariants which define the free energy function. It is believed

that from the computational point of view such a general approach is not practicable since it completely blows up the numerical treatment. Contrary, the proposed framework deals with a reduced but physically motivated set of three invariants leading to manageable numerics. As a main advantage standard isotropic free energy functions are sufficient to model overall anisotropic continuum damage without any further modelling.

Moreover, the well established concept of standard dissipative materials has been applied, in connection with a dissipation potential and associated flow rules. Later on, two types of damage evolution have been introduced, namely quasi-isotropic damage with constant principle damage directions and generally anisotropic damage incorporating evolution of the principle damage directions. Both categories can be coupled with isotropic or anisotropic hyper-elasticity, respectively. Nevertheless, the modelling of specific materials taking into account effects like different behavior for tension and compression and the coupling to anisotropic, large strain plasticity are important areas constituting future research.

Referring to time integration within the proposed rate-independent, staggered formulation different higher order methods have been applied. Since to the knowledge of the authors no exponential scheme concerning the general anisotropic case is conveniently available, Runge–Kutta algorithms have been used for the computation. Thereby, two different schemes were outlined forcing intermediate stages to satisfy the damage condition (2) or not (1), respectively. Within the subsequent numerical examples especially diagonally implicit Runge–Kutta algorithms within integration Scheme 2 render results of satisfying accuracy for large integration intervals. Nevertheless, for the case of coupling hyper-elasticity, continuum damage and plasticity in the light of overall anisotropy at large strains one has additionally eigenvalues due to internal variables which are increasing during the deformation. Thus, it is believed that by taking plasticity into account the accuracy of the applied integration algorithm is of even greater importance than within the given formulation due to continuum damage.

Summarizing, this work gave a framework and an outline of the corresponding numerical treatment of the modelling of overall anisotropic material at large strains incorporating second order internal variables in a thermodynamically consistent way. The identification of material parameters – e.g. for the initialization of the damage metric tensor – is of outstanding importance for future investigations.

Appendix A. Notation of invariants and identity tensors

To set the stage and for convenience of the reader some essential notations which are invoked in this work are summarized in the following:

The characteristic equation for an arbitrary, symmetric, second order tensor $\boldsymbol{A} \in \mathbb{R}^3 \times \mathbb{R}^3$ denoted by $\boldsymbol{A}^3 - {}^A J_1 \boldsymbol{A}^2 + {}^A J_2 \boldsymbol{A} - {}^A J_3 \boldsymbol{I} = \boldsymbol{0}$, whereby $\boldsymbol{I}$ represents the second order identity tensor, defines the principal invariants

$$ {}^A J_1 = \boldsymbol{I}{:}\boldsymbol{A}, \quad {}^A J_2 = \tfrac{1}{2}\left[{}^A J_1^2 - \boldsymbol{I}{:}\boldsymbol{A}^2\right], \quad {}^A J_3 = \det(\boldsymbol{A}). \tag{A.1} $$

Additionally the basic invariants are denoted by

$$ {}^A I_1 = \boldsymbol{I}{:}\boldsymbol{A}^1, \quad {}^A I_2 = \boldsymbol{I}{:}\boldsymbol{A}^2, \quad {}^A I_3 = \boldsymbol{I}{:}\boldsymbol{A}^3, \tag{A.2} $$

and for completeness the derivatives of the principal and basic invariants with respect to their argument read as follows:

$$ \begin{aligned} &\partial_{\boldsymbol{A}} {}^A J_1 = \boldsymbol{I}, && \partial_{\boldsymbol{A}} {}^A I_1 = 1\boldsymbol{A}^0, \\ &\partial_{\boldsymbol{A}} {}^A J_2 = {}^A J_1 \boldsymbol{I} - \boldsymbol{A}, && \partial_{\boldsymbol{A}} {}^A I_2 = 2\boldsymbol{A}^1, \\ &\partial_{\boldsymbol{A}} {}^A J_3 = {}^A J_3 \boldsymbol{A}^{-1} = \operatorname{cof}(\boldsymbol{A}), && \partial_{\boldsymbol{A}} {}^A I_3 = 3\boldsymbol{A}^2. \end{aligned} \tag{A.3} $$

Next, two symmetric, second order tensors $\boldsymbol{O}, \boldsymbol{P} \in \mathbb{R}^n \times \mathbb{R}^n$ are introduced. They define a set of 10 invariants ${}^{OP}\tilde{I}_{1,\ldots,10}$ which is denoted by

$$
\begin{aligned}
&{}^{OP}\tilde{I}_i = \boldsymbol{I} : \boldsymbol{O}^i, \quad {}^{OP}\tilde{I}_j = \boldsymbol{I} : \boldsymbol{P}^{j-3}, \quad {}^{OP}\tilde{I}_7 = \boldsymbol{O} : \boldsymbol{P}, \\
&{}^{OP}\tilde{I}_8 = [\boldsymbol{O} \cdot \boldsymbol{P}] : \boldsymbol{O}, \quad {}^{OP}\tilde{I}_9 = [\boldsymbol{P} \cdot \boldsymbol{O}] : \boldsymbol{P}, \quad {}^{OP}\tilde{I}_{10} = [\boldsymbol{O} \cdot \boldsymbol{P} \cdot \boldsymbol{O}] : \boldsymbol{P},
\end{aligned}
\tag{A.4}
$$

with $i = 1, 2, 3$ and $j = 4, 5, 6$. Furthermore, two non-standard dyadic products $\overline{\otimes}$ and $\underline{\otimes}$ are used. For some arbitrary, second order tensors $\boldsymbol{X}$, $\boldsymbol{Y} \in \mathbb{R}^n \times \mathbb{R}^n$ these dyadics render in index notation with respect to a cartesian frame

$$
[\boldsymbol{X} \overline{\otimes} \boldsymbol{Y}]_{ijkl} = \boldsymbol{X}_{ik} \boldsymbol{Y}_{jl} \quad \text{and} \quad [\boldsymbol{X} \underline{\otimes} \boldsymbol{Y}]_{ijkl} = \boldsymbol{X}_{il} \boldsymbol{Y}_{jk}. \tag{A.5}
$$

Now, besides the standard dyadic product $\boldsymbol{I} \otimes \boldsymbol{I}$ two different fourth-order identity tensors can be formulated

$$
\mathbf{1}^{\mathrm{sym}} = \tfrac{1}{2}[\boldsymbol{I} \overline{\otimes} \boldsymbol{I} + \boldsymbol{I} \underline{\otimes} \boldsymbol{I}] \quad \text{and} \quad \mathbf{1}^{\mathrm{skw}} = \tfrac{1}{2}[\boldsymbol{I} \overline{\otimes} \boldsymbol{I} - \boldsymbol{I} \underline{\otimes} \boldsymbol{I}], \tag{A.6}
$$

constructed by symmetric and skew-symmetric composition of the non-standard dyadic products with respect to the second-order identity tensor.

Usually the free energy function within a material setting due to some non-linear elastic behavior is computed by the principal invariants ${}^{C}J_{1-3}$ with respect to the right Cauchy–Green tensor $\boldsymbol{C}$. The formulation proposed in this work is actually based on the basic invariants ${}^{E}I_{1-3}$ in terms of the Green–Lagrange strain tensor $\boldsymbol{E}$, whereby the one to one relation between these two sets of invariants is given by:

$$
\begin{aligned}
{}^{C}J_1 &= 3 + 2{}^{E}I_1, \\
{}^{C}J_2 &= 3 + 4{}^{E}I_1 - 2{}^{E}I_2 + 2{}^{E}I_1^2, \\
{}^{C}J_3 &= 1 + 2{}^{E}I_1 - 2{}^{E}I_2 + 8/3{}^{E}I_3 + 2{}^{E}I_1^2 - 4{}^{E}I_1{}^{E}I_2 + 4/3{}^{E}I_1^3.
\end{aligned}
\tag{A.7}
$$

Moreover, the heart of the proposed framework to formulate anisotropy lies in the replacement of these invariants, to be specific: $\bar{\Psi} = \bar{\Psi}({}^{\bar{E}\bar{B}}I_i \doteq {}^{\bar{E}}I_i) = \Psi({}^{EB}I_i)$ in $\mathscr{B}_0$ with $i = 1, 2, 3$.

Appendix B. Tensor-valued tensor functions

Let $\boldsymbol{X}$, $\dot{\boldsymbol{X}}$, $\boldsymbol{Y}$, $\boldsymbol{Z} \in \mathbb{R}^n \times \mathbb{R}^n$ denote symmetric, second order tensors which define the tensor-valued tensor function $\dot{\boldsymbol{X}} = \dot{\boldsymbol{X}}(\boldsymbol{Y}, \boldsymbol{Z})$. Furthermore, $\boldsymbol{X}$ and $\boldsymbol{Z}$ represent conjugate variables which would yield within the framework of an associated setting $\dot{\boldsymbol{X}} = \dot{\gamma}\, \partial_{\boldsymbol{Z}} \Phi(\boldsymbol{Y}, \boldsymbol{Z})$ whereby Φ is an assumed dissipation potential and $\dot{\gamma}$ denotes the Lagrange multiplier. Following the outline given in Betten (1985) the general canonical form of this rate equation reads

$$
\dot{\boldsymbol{X}} = \dot{\boldsymbol{X}}(\boldsymbol{Y}, \boldsymbol{Z}) = \sum_{\alpha=0}^{2} {}^{\alpha}\boldsymbol{H} : \boldsymbol{Z}^{\alpha} \quad \text{with} \quad {}^{\alpha}\boldsymbol{H} = \sum_{\beta=0}^{2} \phi_{\alpha,\beta}\, {}^{\beta}\boldsymbol{M} \quad \text{and} \quad {}^{\beta}\boldsymbol{M} = \tfrac{1}{2}\big[\boldsymbol{Y}^{\beta} \overline{\otimes} \boldsymbol{I} + \boldsymbol{Y}^{\beta} \underline{\otimes} \boldsymbol{I}\big]^{\mathrm{sym}}, \tag{B.1}
$$

whereby the nine scalar-valued function $\phi_{\alpha,\beta}$ with $\alpha, \beta = 0, 1, 2$ are generally defined by the corresponding set of 10 invariants; $\phi_{\alpha,\beta} = \phi_{\alpha,\beta}({}^{YZ}\tilde{I}_{1,\ldots,10})$. The assumption of a dissipation potential $\Phi = \Phi(\boldsymbol{Y}, \boldsymbol{Z})$ within an associated setting and in connection with the abbreviation $\Phi_i = \partial_{{}^{YZ}\tilde{I}_i} \Phi$ for $i = 1, \ldots, 10$ yields

$$
\begin{aligned}
&\phi_{0,0} = \dot{\gamma}\Phi_4, \quad \phi_{0,1} = \dot{\gamma}\Phi_7, \quad \phi_{0,2} = \dot{\gamma}\Phi_8, \\
&\phi_{1,0} = \tfrac{1}{2}\dot{\gamma}\Phi_5, \quad \phi_{1,1} = \tfrac{1}{2}\dot{\gamma}\Phi_9, \quad \phi_{1,2} = \tfrac{1}{2}\dot{\gamma}\Phi_{10}, \\
&\phi_{2,0} = \tfrac{1}{3}\dot{\gamma}\Phi_6, \quad \phi_{2,1} = 0, \quad \phi_{2,2} = 0.
\end{aligned}
\tag{B.2}
$$

These relations are one to one with Eq. (17) and obviously represent a restricted form of Eq. (B.1) which is actually based on the fact that ${}^{YZ}\tilde{I}_{1,2,3}$ do not depend on $\boldsymbol{Z} \rightsquigarrow \partial_{\boldsymbol{Z}}\, {}^{YZ}\tilde{I}_{1,2,3} = \mathbf{0}$.

Appendix C. Runge–Kutta schemes

For completeness and convenience of the reader some Runge–Kutta schemes are given in the sequel with respect to the Butcher array, Section 4. Without loss of generality the intermediate points are defined by $c_i = \sum_{j=1}^{s} a_{ij}$ and furthermore all other not mentioned coefficients equal zero. Following standard notation s denotes the stage and p the order of accuracy; see e.g. Lambert (1991) and Ascher and Petzold (1998).

The simplest explicit method (Euler forward, $s = p = 1$) is defined by $b_1 = 1$. Combining several Euler steps ends up in Heun methods, e.g. $s = p = 2$ for $a_{21} = 1$ and $b_1 = b_2 = 1/2$.

Now, three families of implicit Runge–Kutta methods are outlined, Gauss (including the midpoint rule), Radau 2a (Euler backward) and Lobatto 3a (trapezoid method). One considered algorithm of the family of highest possible order – Gauss – for $s = 2$ and $p = 4$ is given by $a_{11} = a_{22} = 1/4$, $a_{12} = (3 - 2\sqrt{3})/12$, $a_{21} = (3 + 2\sqrt{3})/12$ and $b_1 = b_2 = 1/2$. A two stage scheme of the Radau 2a type of order $p = 3$, generally including stiff decay, reads $a_{11} = 5/12$, $a_{12} = -(1/12)$, $a_{21} = b_1 = 3/4$ and $a_{22} = b_2 = 1/4$. From the computational point of view algorithms due to Lobatto 3a are less expensive than expressed by their stage s since the first intermediate state t_1 coincides with the known one of ${}^{n}t$. For $s = 3$ and $p = 4$ one has $a_{21} = 5/24$, $a_{22} = 1/3$, $a_{23} = -1/24$, $a_{31} = b_1 = a_{33} = b_3 = 1/6$ and $a_{32} = b_2 = 2/3$.

Finally, diagonally implicit Runge–Kutta methods (DIRK) are numerically interesting since they do not blow up the system of equations within the Newton iteration, see Eq. (23). A two stage Gauss DIRK scheme with $p = 3$ is constructed by $a_{11} = a_{22} = \alpha_G$, $a_{22} = 1 - 2\alpha_G$ and $b_1 = b_2 = 1/2$ with $\alpha_G = (3 + \sqrt{3})/6$. Similar the Radau 2a DIRK algorithm for $s = 2$ and order $p = 2$ takes the form $a_{11} = a_{22} = b_2 = \alpha_R$ and $a_{21} = b_1 = 1 - \alpha_R$ with $\alpha_R = (2 - \sqrt{2})/2$.

References

Altmann, S.L., 1986. Rotations, Quaternions and Double Groups, Oxford University Press.

Ascher, U.M., Petzold, L.R., 1998. Computer Methods for Ordinary Differential Equations and Differential–Algebraic Equations, SIAM.

Betten, J., 1982. Theory of invariants. In: Boehler, J.P. (Ed.), Creep Mechanics of Anisotropic Materials, Mechanical Behaviour of Anisotropic Materials, EUROMECH Colloquium 115, Grenoble, 1979. Martinus Nijhoff Publishers, pp. 65–80.

Betten, J., 1985. The classical plastic potential theory in comparison with the tensor function theory. Engng. Fract. Mech. 21 (4), 641–652.

Betten, J., 1988. Application of tensor functions to the formulation of yield criteria for anisotropic materials. Int. J. Plasticity 4, 29–46.

Betten, J., 1991. Recent advances in applications of tensor functions in solid mechanics. Adv. Mech. 14 (1), 79–109.

Betten, J., 1992. Application of tensor functions in continuum damage mechanics. Int. J. Damage Mech. 1, 47–59.

Betten, J., Sklepus, S., Zolochevsky, A., 1998. A creep damage model for initially isotropic materials with different properties in tension and compression. Engng. Fract. Mech. 59 (5), 623–641.

Boehler, J.P., 1987. Applications of tensor functions in solid mechanics. CISM courses and lectures, no. 292. Springer, Berlin.

Boehler, J.P., Sawczuk, A., 1976. Application of representation theorems to describe yielding of transversely isotropic solids. Mech. Res. Commun. 3, 277–283.

Carol, I., Rizzi, E., Willam, K., 2001a. On the formulation of anisotropic elastic degradation. I. Theory based on a pseudo-logarithmic damage tensor rate. Int. J. Solids Struct. 38, 491–518.

Carol, I., Rizzi, E., Willam, K., 2001b. On the formulation of anisotropic elastic degradation. II. Generalized pseudo-Rankine model for tensile damage. Int. J. Solids Struct. 38, 519–546.

Chaboche, J.-L., 1993. Development of continuum damage mechanics for elastic solids substaining anisotropic and unilateral damage. Int. J. Damage Mech. 2, 311–329.

Diebels, S., Ellsiepen, P., Ehlers, W., 1998. Error-controlled Runge–Kutta time integration of a viscoplastic hybrid two-phase model. Tech. Mech. 19 (1), 19–27.

Engeln-Müllges, G., Uhlig, F., 1996. Numerical Algorithms with FORTRAN. Springer, Berlin.

Hackl, K., 1998. A Survey on time-integration algorithms for convex and nonconvex elastoplasticity. In: Gilbert, R.G., et al. (Eds.), From Convexity to Nonconvexity, Nonsmooth Optimization and its Applications. Kluwer, Dordrecht.

Halphen, B., Nguyen, Q.S., 1975. Sur les Matériaux Standards Généralisés. Jounal de Mecanique 14, 39–62.

Kirchner, E., Kollmann, F.G., 1999. Application of modern time integrators to Hart's model. Int. J. Plasticity 15 (6), 647–666.
Lambert, J.D., 1991. Numerical Methods for Ordinary Differential Systems: The Initial Value Problem. Wiley, New York.
Leckie, F.A., Onat, E.T., 1981. Tensorial nature of damage measuring internal variables. In: Hult, J., Lemaitre, J. (Eds.), Physical Non-Linearities in Structural Analysis, IUTAM Symposium Senlis/France, 1980. Springer, Berlin, pp. 140–155.
Lemaitre, J., Chaboche, J.-L., 1998. Mechanics of Solid Materials, second paperback edition, Cambridge, University Press.
Matzenmiller, A., Sackman, J.L., 1994. On damage induced anisotropy for fiber composites. Int. J. Damage Mech. 3, 71–86.
Menzel, A., Steinmann, P., 1999. A theoretical and computational setting for geometrically nonlinear damage mechanics. In: Wunderlich, W. (Ed.), Proceedings of the European Conference on Computational Mechanics ECCM, no. 329.
Miehe, C., 1995. Discontinuous and continuous damage evolution in Ogden-type large-strain elastic materials. Eur. J. Mech., A/Solids 14 (5), 697–720.
Miehe, C., 1998. A constitutive frame of elastoplasticity at large strains based on the notion of a plastic metric. Int. J. Solids Struct. 35 (30), 3859–3897.
Murakami, S., 1987. Anisotropic aspects of material damage and application of continuum damage mechanics. In: Krajcinovic, D., Lemaitre, J. (Eds.), Continuum Damage Mechanics, CISM Courses and Lectures, no. 295. Springer, Berlin.
Murakami, S., 1988. Mechanical modeling of material damage. ASME J. Appl. Mech. 55, 280–286.
Ogden, R.W., 1997. Non-Linear Elastic Deformations, Dover, New York.
Park, T., Voyiadjis, G.Z., 1998. Kinematic description of damage, ASME J. Appl. Mech. 65, 93–98.
Sansour, C., 1999. The dual variable of the Cauchy stress tensor and the geometry of deformations. Preprint.
Schreyer, H.L., 1995. Continuum damage based on elastic projection tensors, Int. J. Damage Mech. 4, 171–195.
Simo, J.C., 1998. Numerical analysis and simulation of plasticity. In: Ciarlet, P.G., Lions, J.L. (Eds.), Numerical Methods for Solids (Part 3), Handbook of Numerical Analysis, vol. 6. North-Holland, Amsterdam.
Smith, G.F., 1994. Constitutive Equations for Anisotropic and Isotropic Materials, Mechanics and Physics of Discrete Systems, vol. 3. North-Holland, Amsterdam.
Spencer, A.J.M., 1971. Theory of invariants. In: Eringen, A.C. (Ed.), Continuum Physics, vol. 1. Academic Press, New York.
Spencer, A.J.M., 1984. Constitutive theory of strongly anisotropic solids. In: Spencer, A.J.M. (Ed.), Continuum Theory of the Mechanics of Fibre-Reinforced Composites, CISM Courses and Lectures, no. 282. Springer, Berlin.
Steinmann, P., Carol, I., 1998. A framework for geometrically nonlinear continuum damage mechanics. Int. J. Engng. Sci. 36, 1793–1814.
Svendsen, B., 2001. On the modeling of anisotropic elastic and inelastic material behaviour at large deformation. Int. J. Solids Struct. 38, 9579–9599.
Weber, G., Anand, L., 1990. Finite deformation constitutive equations and a time integration procedure for isotropic, hyperelastic-viscoplastic solids. Comp. Meth. Appl. Mech. Engng. 79, 173–202.